HOKKAIDO UNIVERSITY

Title	Electric field thermopower modulation analyses of the operation mechanism of transparent amorphous SnO2 thin-film transistor
Author(s)	Liang, Dou-dou; Zhang, Yu-qiao; Cho, Hai Jun; Ohta, Hiromichi
Citation	Applied physics letters, 116(14), 143503 https://doi.org/10.1063/5.0003153
Issue Date	2020-04-06
Doc URL	http://hdl.handle.net/2115/80828
Rights	This article may be downloaded for personal use only. Any other use requires prior permission of the author and AIP Publishing. This article appeared in Liang Dou-dou, Zhang Yu-qiao, Cho Hai Jun, Ohta Hiromichi. Electric field thermopower modulation analyses of the operation mechanism of transparent amorphous SnO2 thin-film transistor. Applied physics letters, 116, 143503 (2020) and may be found at https://doi.org/10.1063/5.0003153 .
Type	article
File Information	5.0003153.pdf

Hokkaido University Collection of Scholarly and Academic Papers : HUSCAP

Applied Physics Letters

Electric field thermopower modulation analyses of the operation mechanism of transparent amorphous SnO_2 thin-film transistor

Cite as: Appl. Phys. Lett. **116**, 143503 (2020); https://doi.org/10.1063/5.0003153
Submitted: 30 January 2020 . Accepted: 22 March 2020 . Published Online: 07 April 2020

Dou-dou Liang, Yu-qiao Zhang, Hai Jun Cho, and Hiromichi Ohta

ARTICLES YOU MAY BE INTERESTED IN

Solution-processed ITO thin-film transistors with doping of gallium oxide show high on-off ratios and work at 1 mV drain voltage
Applied Physics Letters **116**, 141604 (2020); https://doi.org/10.1063/1.5141140

Scaling-down and interfacial effect to break down the trade-off between thermal stability and crystallization speed of the Sb_2Se films
Applied Physics Letters **116**, 141601 (2020); https://doi.org/10.1063/1.5143060

High electrical conducting deep-ultraviolet-transparent oxide semiconductor La-doped $SrSnO_3$ exceeding ~3000 S cm^{-1}
Applied Physics Letters **116**, 022103 (2020); https://doi.org/10.1063/1.5128410

Lock-in Amplifiers up to 600 MHz

© 2020 Author(s).

Electric field thermopower modulation analyses of the operation mechanism of transparent amorphous SnO_2 thin-film transistor

Cite as: Appl. Phys. Lett. **116**, 143503 (2020); doi: 10.1063/5.0003153
Submitted: 30 January 2020 · Accepted: 22 March 2020 ·
Published Online: 7 April 2020

View Online

Export Citation

CrossMark

Dou-dou Liang,[1,2,a)] Yu-qiao Zhang,[2] Hai Jun Cho,[2] and Hiromichi Ohta[2,a)]

AFFILIATIONS

[1]The Beijing Municipal Key Laboratory of New Energy Materials and Technologies, School of Materials Science and Engineering, University of Science and Technology Beijing, Beijing 100083, China
[2]Research Institute for Electronic Science, Hokkaido University, N20W10, Kita, Sapporo 001-0020, Japan

[a)]Authors to whom correspondence should be addressed: liangdoudou1993@foxmail.com and hiromichi.ohta@es.hokudai.ac.jp

ABSTRACT

Transparent amorphous oxide semiconductors (TAOSs) based transparent thin-film transistors (TTFTs) with high field effect mobility (μ_{FE}) are essential for developing advanced flat panel displays. Among TAOSs, amorphous (a-) SnO_2 has several advantages against current a-$InGaZnO_4$ such as higher μ_{FE} and being indium-free. Although a-SnO_2 TTFT has been demonstrated several times, the operation mechanism has not been clarified thus far due to the strong gas sensing characteristics of SnO_2. Here we clarify the operation mechanism of a-SnO_2 TTFT by electric field thermopower modulation analyses. We prepared a bottom-gate top-contact type TTFT using 4.2-nm-thick a-SnO_2 as the channel without any surface passivation. The effective thickness of the conducting channel was $\sim$1.7 $\pm$ 0.4 nm in air and in vacuum, but a large threshold gate voltage shift occurred in different atmospheres; this is attributed to carrier depletion near at the top surface ($\sim$2.5 nm) of the a-SnO_2 due to its interaction with the gas molecules and the resulting shift in the Fermi energy. The present results would provide a fundamental design concept to develop a-SnO_2 TTFT.

Published under license by AIP Publishing. https://doi.org/10.1063/5.0003153

Transparent amorphous oxide semiconductors (TAOSs) based transparent thin-film transistors (TTFTs) with high field effect mobility (μ_{FE}) are essential components for advanced flat panel displays such as transparent organic light-emitting diode (OLED) displays and rollable OLED displays. Currently, amorphous (a-) $InGaZnO_4$ is widely applied as the TAOS[1–4] of the TFT channel of commercially available OLED displays; the optical bandgap of a-$InGaZnO_4$ is $\sim$3 eV,[5] transparent in the visible light region, and the μ_{FE} of a-$InGaZnO_4$ ($\sim$10 cm^2 V^{-1} s^{-1}[1,2]) is two orders of magnitude higher than that of previously used a-Si. However, the use of a-$InGaZnO_4$ must be reduced because the consumption of rare element such as indium (Clarke number: 1×10^{-5}%) is not desirable for maintaining sustainable usage of resources. Therefore, development of post-a-$InGaZnO_4$ TAOSs showing high μ_{FE}, which are composed of abundant elements, is crucial.

Among several indium-free TAOSs,[6–8] a-SnO_2 is a promising candidate for overcoming the issues with a-$InGaZnO_4$. Sn is one of the abundant metal elements with the Clarke number[9] of Sn which is 4×10^{-3}%, 400 times larger than that of In. Moreover, SnO_2 TFT shows extremely high $\mu_{FE} > 100$ cm^2 V^{-1} s^{-1},[10–12] which is one order of magnitude higher than that of a-$InGaZnO_4$. In 2007, Dattoli *et al.*[10] reported that Ta-doped SnO_2 nanowire TFT exhibits uniform characteristics with average μ_{FE} exceeding 100 cm^2 V^{-1} s^{-1} at room temperature. In 2009, Sun *et al.*[11] fabricated Sb-doped SnO_2 nanocrystal TFTs at room temperature with μ_{FE} of 158 cm^2 V^{-1} s^{-1}. In 2016, Shin *et al.*[12] reported that an extremely thin (<4.5 nm) undoped SnO_2 TFT exhibited μ_{FE} of 150 cm^2 V^{-1} s^{-1} at room temperature in air. In these reports, bottom-gate top-contact type TFTs without any passivation showed high μ_{FE}. Thus, the top surface of SnO_2 channel was exposed to the atmosphere.

SnO_2 is a well-known gas sensing material.[13,14] It is known that a 3–4-nm-thick depletion layer is formed at the SnO_2 surface.[15,16] Oxygen molecules in the ambient atmosphere are adsorbed on the surface, seize free electrons near the surface, and form a depletion layer. In a reducing atmosphere, parts of the seized electrons are released back to the depletion layer. Thus, the transistor characteristics of the bottom-gate top-contact type SnO_2 TFTs would be strongly affected by the gases surrounding the exposed channel surface due to their gas sensing property. For this reason, the operation mechanism of the bottom-gate

top-contact type SnO_2 TFTs including the conduction band bending and the effective channel thickness have not been clarified thus far.

Here we clarify the conduction band bending and the effective channel thickness of 4.2-nm-thick a-SnO_2 based bottom-gate top-contact type TTFTs without any surface passivation. We analyzed the conduction band bending of the SnO_2 top surface by measuring the TFT characteristics in air and vacuum, and a large threshold gate voltage shift was observed; the Fermi energy in the carrier depletion region at the top surface (~2.5 nm) of the a-SnO_2 channel sensitively shifted with the changes in the gas atmosphere. The effective channel thickness (t_{eff}) was analyzed by the electric field thermopower (S) modulation method,,[17–21] and the t_{eff} was $\sim 1.7 \pm 0.4$ nm in air and in vacuum. The present results would provide a fundamental design concept for developing a-SnO_2 TTFT.

The bottom-gate top-contact TTFTs (Fig. 1) were fabricated on 100-nm-thick ITO coated alkali-free glass (thickness: 0.7 mm, Corning® EAGLE XG®) substrates by pulsed laser deposition (PLD, KrF excimer laser, 10 Hz) technique. First, a 300-nm-thick polycrystalline Y_2O_3 gate dielectric film (the dielectric permittivity, $\varepsilon_r = 20$[22]) was deposited at room temperature. The fluence of the KrF laser was ~2 J cm^{-2} $pulse^{-1}$, and the oxygen pressure was kept at 0.4 Pa during deposition. Then, a 4.2-nm-thick SnO_2 film was deposited on the Y_2O_3/ITO bilayer laminate through a stencil mask at 300 °C [see supplementary material Figs. S1(a) and S1(b)]. The fluence of the KrF laser was ~0.3 J cm^{-2} $pulse^{-1}$, and the oxygen pressure was kept at 1 Pa during the deposition. The optical bandgap (E_g) of the a-SnO_2 film was ~4.3 eV [supplementary material Fig. S1(c)], which was larger than that of bulk SnO_2 ($E_g \sim 3.6$ eV).[23] This is most likely due to the quantum size effect.[24] Finally, 100-nm-thick ITO films, which were used as the source and drain electrodes (400 μm × 400 μm), were deposited at room temperature. The fluence of the KrF laser was ~0.9 J cm^{-2} $pulse^{-1}$ and the oxygen pressure was kept at 3 Pa during deposition. After these PLD processes, the device was annealed at 400 °C for 30 min in air. The channel length L and the channel width W of the resultant TFT were 200 and 400 μm, respectively. The resultant multiple layer was fully transparent in the visible light region (supplementary material Fig. S2).

The TTFT characteristics such as transfer characteristics (I_d–V_g) and output characteristics (I_d–V_d) were measured using a semiconductor device analyzer (B1500A, Agilent Co.) at room temperature. As shown in Fig. 2(a), the resultant TTFTs showed clear transfer (I_d–V_g) characteristics with the on-to-off current ratios of $\sim 10^5$. All the TFTs show clear pinch-off in the output characteristics [supplementary material Fig. S3], indicating that the TFT operation obeys the standard field-effect theory. It should be noted that the threshold gate voltage (V_{th}), which was evaluated by plotting $I_d^{0.5}$–V_g relationship, was −14 V in air but shifted dramatically to −23 V in vacuum. The μ_{FE}, calculated from $\mu_{FE} = g_m \cdot [(W/L) \cdot C_i \cdot V_d]^{-1}$, where g_m is the transconductance $\partial I_d / \partial V_g$ and C_i is capacitance per unit area (C_i ~58 nF cm^{-2}),[22] was ~20 cm^2 V^{-1} s^{-1} in air and ~30 cm^2 V^{-1} s^{-1} in vacuum. These confirm that the channel conductance and the V_{th} indeed can be modulated with the gases surrounding exposed a-SnO_2 channel. The SnO_2 TTFT characteristics were summarized in Table I.

The electric field modulated thermopower (S) was measured during the transfer characteristics measurements in the two gas

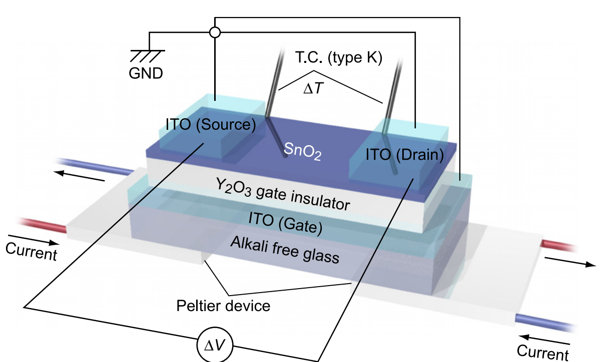

FIG. 1. Electric field thermopower modulation measurement of the bottom-gate top-contact a-SnO_2 TTFT. The top surface of the 4.2-nm-thick SnO_2 channel is exposed to the air. The channel length L is 200 μm and the channel width W is 400 μm. The gate insulator is 300-nm-thick polycrystalline Y_2O_3 ($\varepsilon_r = 20$). The SnO_2 channel is placed on the gap (~2 mm) between two Peltier devices, which are used to give temperature difference (ΔT) between both edges of the channel. Two K-type thermocouples (T.C.) are located at both edges of the SnO_2 channel to measure the temperature difference between both edges of the SnO_2 channel. The thermoelectromotive force (ΔV) and ΔT are measured simultaneously at a fixed gate voltage (V_g).

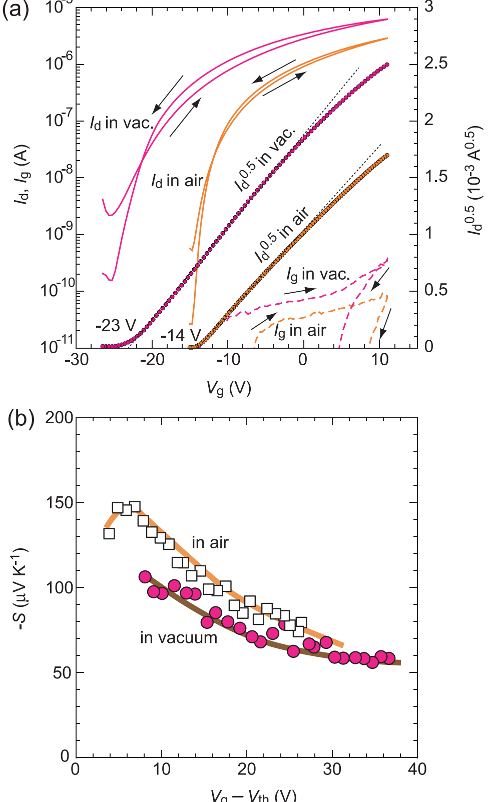

FIG. 2. Transistor characteristics the bottom-gate top-contact a-SnO_2 TTFT measured in air and in vacuum. (a) Transfer characteristic (I_d–V_g) curve at V_d = +0.1 V. Corresponding $I_d^{0.5}$–V_g and I_g–V_g curves are also shown. The threshold voltage (V_{th}) is −14 V in air and −23 V in vacuum. The gate leakage current (I_g) is < 100 pA. (b) Electric field modulated thermopower (S) at various V_g–V_{th} ranging from +4 V to +37 V. The $-S$ gradually decreases with V_g–V_{th}.

Published under license by AIP Publishing

TABLE I. On-ff current ratio, threshold gate voltage (V_{th}), subthreshold swing factor ($S.S.$), and field effect mobility (μ_{FE}) for SnO_2 TTFT.

	ON/OFF	V_{th} (V)	$S.S.$ (V decade^{-1})	μ_{FEmax} (cm^2 V^{-1} s^{-1})
Air	$\sim 10^5$	-14	0.65 ± 0.02	20
Vacuum	$\sim 10^5$	-23	1.57 ± 0.2	30

atmospheres (air, vacuum) to analyze the t_{eff}. Details of the electric field modulated S measurement are described elsewhere.[17–20] Figure 2(b) shows the changes in $-S$ as a function of the effective gate voltage ($V_g - V_{th}$). The S values were always negative, consistent with the fact that the SnO_2 film is n-type semiconductor. The absolute values of S decrease gradually with increasing $V_g - V_{th}$ in both atmospheres due to an increase in the sheet carrier concentration (n_s), which was deduced from $n_s = C_i \cdot (V_g - V_{th}) \cdot e^{-1}$. Although a small variation in S was observed due to the gate leakage current (I_g), the observed S could be used to analyze the t_{eff} since the variation is less than 10%, and the difference in the air and vacuum atmospheres is noticeably clear.

In order to extract the t_{eff}, we plotted $-S$ as a function of n_s [Fig. 3(a)]. An almost linear relationship with a slope of $\sim$120 μV K^{-1} decade^{-1} was observed in the $-S$ vs log n_s plot when n_s exceeded 2.5×10^{12} cm^{-2} in air, and a slope of $\sim$84 μV K^{-1} decade^{-1} was observed in the same plot when n_s exceeded 2.9×10^{12} cm^{-2} in vacuum. We also plotted the three-dimensional carrier concentration (n_{3D}) dependence of $-S$ measured from separately prepared SnO_2 thin films [Fig. 3(b), Table S1]. From the $-S$ vs log n_{3D} relationship, the carrier effective mass (m^*) of the SnO_2 films was extracted to be 0.47 m_0 using the following equations:

$$s = \frac{k_B}{e}\left(\frac{\left(r+\frac{5}{2}\right)F_{\left(r+\frac{3}{2}\right)}(\eta)}{\left(r+\frac{3}{2}\right)F_{\left(r+\frac{1}{2}\right)}(\eta)} - \eta\right), \tag{1}$$

$$n_H = \frac{1}{eR_H} = \frac{8\pi\left(2m_d^* k_B T\right)^{\frac{3}{2}}}{3h^3}\frac{\left(r+\frac{3}{2}\right)^2 F^2{}_{\left(r+\frac{1}{2}\right)}(\eta)}{\left(2r+\frac{3}{2}\right)F_{\left(2r+\frac{1}{2}\right)}(\eta)}, \tag{2}$$

$$F_n(\eta) = \int_0^\infty \frac{x^n}{1+e^{x-\eta}}dx, \tag{3}$$

where $F_n(\eta)$ is the nth order Fermi integral, η is the reduced fermi energy, r is the scattering factor, h is the Planck constant, and k_B is the Boltzmann constant. Because acoustic phonon scattering is commonly the main scattering mechanism for this material, the scattering factor r could be considered as $-1/2$. S only depends on the slope of the electronic density of states at the Fermi level, which depends on n_{3D}. Since the n_s measured from the transistor characteristics represents the projected n_{3D} within the t_{eff}, we can directly compare the $-S$ vs log n_s relationship with the $-S$ vs log n_{3D} relationship. The slope of $-S$ vs log n_{3D} plot [Fig. 3(b)] is comparable to that of the $-S$ vs log n_s plot [Fig. 3(a)], indicating that the $E-k$ relation at the bottom of the conduction band is parabolic, and t_{eff} can be extracted as n_s/n_{3D}.

Several S-values around the lower n_s did not follow the straight line, probably due to that the non-parabolic shaped tail states just below the original conduction band bottom.[18,22,25] The S and n_s were modulated from (–150 μV K^{-1}, 2×10^{12} cm^{-2}) to (–80 μV K^{-1}, 1×10^{13} cm^{-2}) in air and from (–110 μV K^{-1}, 2.9×10^{12} cm^{-2}) to (–60 μV K^{-1}, 1.3×10^{13} cm^{-2}) in vacuum with increasing positive electric field in the a-SnO_2 channel. The difference between the measurements in air and in vacuum is attributed to the gas sensing property of SnO_2, where O_2 molecules are adsorbed in air and released in vacuum. The $t_{eff} \equiv n_s/n_{3D}$ of the conducting a-SnO_2 channel were always $\sim 1.7 \pm 0.4$ nm, insensitive to the gas atmosphere [Fig. 3(c)].

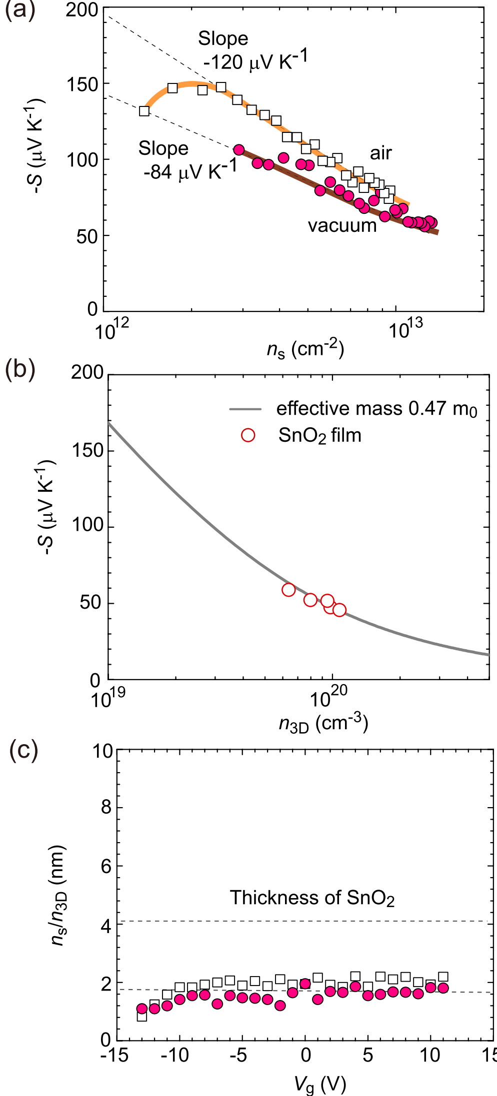

FIG. 3. Electric field thermopower modulation analyses of the bottom-gate top-contact a-SnO_2 TTFT. (a) Change in $-S$ as a function of the sheet carrier concentration (n_s). The slope of the $-S$–n_s relationship is -120 μV K^{-1} decade^{-1} in air and -84 μV K^{-1} decade^{-1} in vacuum (dotted line). (b) Three-dimensional carrier concentration (n_{3D}) dependence S of the SnO_2 films. We calculated the carrier effective mass (m^*) of the SnO_2 film around 0.47 m_0. (c) The effective thickness (t_{eff}), which is defined as n_s/n_{3D}, as a function of V_g. The t_{eff} is always $\sim 1.7 \pm 0.4$ nm, insensitive to the atmosphere.

Published under license by AIP Publishing

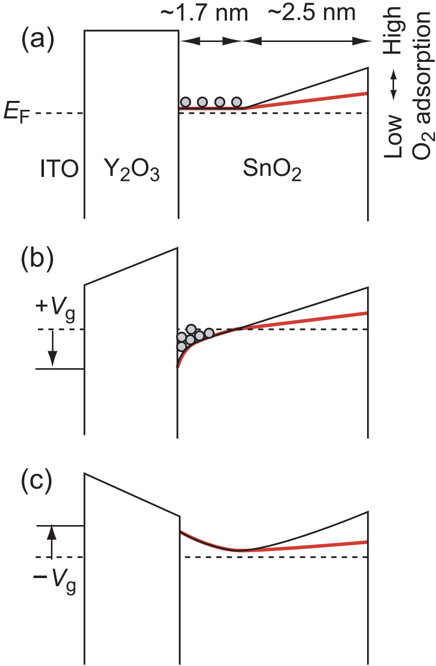

FIG. 4. Electric field modulation mechanism of the bottom-gate top-contact a-SnO_2 TTFT. (a) Without any gate voltage (V_g) application. Conduction band minimum (CBM) around the surface is lifted due to oxygen gas adsorption. Black: higher oxygen atmosphere (air). Red: lower oxygen atmosphere (vacuum). The 2.5-nm-thick surface region is the surface depletion layer. The conducting channel (~1 nm) remains at the Y_2O_3/SnO_2 interface. The sheet carrier concentration (n_s) is $\sim 4 \times 10^{12}\,cm^{-2}$. (b) Under positive V_g application. The 1.7-nm-thick 2DEG layer is formed at the Y_2O_3/SnO_2 interface. The n_s increases up to $\sim 1 \times 10^{13}\,cm^{-2}$. The surface region does not change. (c) Under negative V_g application, the interface electrons are completely depleted, resulting in off states.

Here, we would like to discuss the operation mechanism of a-SnO_2 TTFT [Fig. 4]. Without any V_g application [Fig. 4(a)], the conduction band minimum (CBM) at the surface is lifted due to the adsorption of oxygen when the TTFT is exposed to air (higher oxygen atmosphere, black line). When the TTFT is exposed to vacuum, the CBM at the surface is lowered (lower oxygen atmosphere, red line). Due to the oxygen adsorption, a 2.5-nm-thick depletion layer, which is similar to the Debye length of SnO_2 (~3 nm),[26] is formed near the surface region. As a result, a conducting channel ($\sim 1.7 \pm 0.4$ nm) remains at the Y_2O_3/a-SnO_2 interface, and the n_s is $\sim 4 \times 10^{12}\,cm^{-2}$ ($n_{3D} \sim 2 \times 10^{19}\,cm^{-3}$). Under positive V_g application [Fig. 4(b)], the carriers accumulate at the Y_2O_3/a-SnO_2 interface, and the E_F locates above the CBM. As a result, the 1.7-nm-thick 2D electron gas (2DEG) is formed at the Y_2O_3/a-SnO_2 interface. The n_s increases up to $\sim 1 \times 10^{13}\,cm^{-2}$ ($n_{3D} \sim 4 \times 10^{19}\,cm^{-3}$). The surface region does not change. Under negative V_g application [Fig. 4(c)], the conduction electrons at the Y_2O_3/a-SnO_2 interface are completely depleted, showing off states in the transistor characteristics.

In summary, we have clarified the operation mechanism including the conduction band bending and the effective channel thickness (t_{eff}) of 4.2-nm-thick a-SnO_2 based bottom-gate top-contact type TTFTs without any surface passivation. We analyzed the conduction band bending of SnO_2 top surface by measuring the TFT characteristics in air as well as in vacuum and found the large threshold gate voltage shift; the Fermi energy in the carrier depletion region at the top surface (~2.5 nm) of the a-SnO_2 sensitively shifted depending on the gas atmospheres. We also analyzed the t_{eff} ($\equiv n_s/n_{3D}$) by the electric field thermopower modulation method. t_{eff} was $\sim 1.7 \pm 0.4$ nm in air and in vacuum.

From the thickness of the a-SnO_2 film (4.2 nm) and the t_{eff} (1.7 ± 0.4 nm), the carrier depletion depth at the top surface of the a-SnO_2 film is estimated to be 2.5 nm, which is similar to the depletion length reported in other studies.[15,16] When a-SnO_2 bottom-gate top-contact TTFTs are exposed to air, oxygen gas would be adsorbed on the surface of SnO_2 film as electron accepting species, which is accompanied by the formation of a depletion layer inside the film. The present results may provide a fundamental design concept for utilizing a-SnO_2 TFT in device applications.

See the supplementary material for additional crystallographic analyses of the SnO_2 thin film, optical transmission of the bottom-gate top-contact a-SnO_2 TTFT, transistor characteristics of the bottom-gate top-contact a-SnO_2 TTFT, and optical absorption spectrum of the polycrystalline Y_2O_3 thin film deposited on the SiO_2 glass substrate.

This research was supported by Grants-in-Aid for Innovative Areas (No. 19H05791) and Scientific Research A (No. 17H01314) from the JSPS. D.L. greatly appreciates the support from China Scholarships Council (No. 201806460051). Y.Z. acknowledges the support from Grant-in-Aid for JSPS Fellows (No. 19F1904909) from the JSPS. H.J.C. acknowledges the support from Nippon Sheet Glass Foundation for Materials Science and Engineering. H.O. acknowledges the support from the Asahi Glass Foundation and the Mitsubishi Foundation. A part of this work was also supported by Dynamic Alliance for Open Innovation Bridging Human, Environment, and Materials, and by the Network Joint Research Center for Materials and Devices.

REFERENCES

[1] K. Nomura, H. Ohta, A. Takagi, T. Kamiya, M. Hirano, and H. Hosono, Nature **432**, 488 (2004).
[2] K. Nomura, A. Takagi, T. Kamiya, H. Ohta, M. Hirano, and H. Hosono, Jpn. J. Appl. Phys., Part 1 **45**, 4303 (2006).
[3] T. Kamiya and H. Hosono, Npg Asia Mater. **2**, 15 (2010).
[4] H. Hosono, Nat. Electron. **1**, 428 (2018).
[5] M. Orita, H. Ohta, M. Hirano, S. Narushima, and H. Hosono, Philos. Mag. B **81**, 501 (2001).
[6] P. Gorrn, M. Sander, J. Meyer, M. Kroger, E. Becker, H. H. Johannes, W. Kowalsky, and T. Riedl, Adv. Mater. **18**, 738 (2006).
[7] D. Jousse, C. Constantino, and I. Chambouleyron, J. Appl. Phys. **54**, 431 (1983).
[8] S. H. Sim, K. T. Kang, S. Lee, M. Lee, H. Taniguchi, S. Kim, S. Roh, J. H. Oh, S. A. Lee, J.-S. Bae, J. H. Jang, J. Hwang, S. Han, T. Park, and W. S. Choi, Chem. Mater. **31**, 8019 (2019).
[9] F. W. Clarke and H. S. Washington, *The Composition of the Earth's Crust* (U.S. Government Printing Office, 1924).
[10] E. N. Dattoli, Q. Wan, W. Guo, Y. B. Chen, X. Q. Pan, and W. Lu, Nano Lett. **7**, 2463 (2007).
[11] J. Sun, A. X. Lu, L. P. Wang, Y. Hu, and Q. Wan, Nanotechnology **20**, 335204 (2009).
[12] C. W. Shin, A. Chin, C. F. Lu, and W. F. Su, Sci. Rep. **6**, 19023 (2016).
[13] D. H. Kim, W. S. Kim, S. B. Lee, and S. H. Hong, Sens. Actuators, B **147**, 653 (2010).
[14] S. Das and V. Jayaraman, Prog. Mater. Sci. **66**, 112 (2014).
[15] N. Yamazoe, Sens. Actuators, B **5**, 7 (1991).
[16] V. Lantto, T. T. Rantala, and T. S. Rantala, J. Eur. Ceram. Soc. **21**, 1961 (2001).

Published under license by AIP Publishing

[17] A. V. Sanchela, M. Wei, H. J. Cho, and H. Ohta, Small **15**, 1805394 (2019).
[18] A. V. Sanchela, T. Onozato, B. Feng, Y. Ikuhara, and H. Ohta, Phys. Rev. Mater. **1**, 034603 (2017).
[19] H. Ohta, T. Mizuno, S. J. Zheng, T. Kato, Y. Ikuhara, K. Abe, H. Kumomi, K. Nomura, and H. Hosono, Adv. Mater. **24**, 740 (2012).
[20] H. Ohta, Y. Masuoka, R. Asahi, T. Kato, Y. Ikuhara, K. Nomura, and H. Hosono, Appl. Phys. Lett. **95**, 113505 (2009).
[21] H. Ohta, S. W. Kim, S. Kaneki, A. Yamamoto, and T. Hashizume, Adv. Sci. **5**, 1700696 (2018).
[22] H. Koide, Y. Nagao, K. Koumoto, Y. Takasaki, T. Umemura, T. Kato, Y. Ikuhara, and H. Ohta, Appl. Phys. Lett. **97**, 182105 (2010).
[23] K. Reimann and M. Steube, Solid State Commun. **105**, 649 (1998).
[24] M. B. Sahana, C. Sudakar, A. Dixit, J. S. Thakur, R. Naik, and V. M. Naik, Acta Mater. **60**, 1072 (2012).
[25] Y. Nagao, A. Yoshikawa, K. Koumoto, T. Kato, Y. Ikuhara, and H. Ohta, Appl. Phys. Lett. **97**, 172112 (2010).
[26] K. D. Schierbaum, U. Weimar, W. Gopel, and R. Kowalkowski, Sens. Actuators, B **3**, 205 (1991).

Published under license by AIP Publishing